*J. Fluid Mech.* (1984), *vol.* 139, *pp.* 347–361
*Printed in Great Britain*



# A turbulent mixing layer constrained by a solid surface. Part 2. Measurements in the wall-bounded flow

By D. H. WOOD† AND P. BRADSHAW
Department of Aeronautics, Imperial College, London

(Received 15 May 1983)

The single- and two-point measurements made in a high-Reynolds-number single-stream mixing layer growing to encounter a wind-tunnel floor on its *high-velocity* side that were described by Wood & Bradshaw (1982) have been extended to the wall-bounded flow. It is shown that the expected large amplification of the normal-stress components in the plane of the wall does not occur until after the mixing layer reaches the surface. There is some evidence that the double-roller component of the large-eddy structure of the original free shear layer is being re-established in the wall-bounded flow after having been stretched and weakened by the initial effect of the wall. The triple-product terms appearing in the turbulent-energy and shear-stress equations are altered in a way that cannot be reproduced by models used in current calculation methods. It appears that all the pressure-fluctuation terms in the individual normal-stress and shear-stress transport equations respond in a non-monotonic manner to the imposition of the wall. The implications for calculation methods suitable for predicting the change from an initially unaffected free shear layer to a wall-bounded flow are discussed.

## 1. Introduction

This paper is one of a series on 'complex' turbulent flows, defined as shear layers with complicating influences like distortion by extra rates of strain or interaction with another turbulent field. General reviews of complex flows are given by Bradshaw (1975, 1976). Specifically this paper is a sequel to Wood & Bradshaw (1982; hereinafter cited as I), who made extensive measurements in the initially 'unbounded' single-stream mixing layer shown in figure 1 as it became increasingly influenced by the wind-tunnel floor. The measurements in I were limited to the regions before the mixing layer proper had reached the flow; here we present measurements from the wall-bounded 'mixing layer'.‡ For brevity we will assume that the reader has access to I, where the sparse literature on wall effect is reviewed, and the unbounded large-eddy structure (Grant 1958; also Savill in Kline, Cantwell & Lilley 1982, pp. 999–1004) is shown to be essentially three-dimensional. The conjectured structure is a combination of Grant's 'double-roller eddy' and an 'outer motion' that closes the vortex loop near the potential core, giving the appearance of a horseshoe vortex. As

† Present address: Department of Mechanical Engineering, University of Newcastle, N.S.W. 2308, Australia.

‡ In the absence of a suitable alternative we will continue to describe the flow as a mixing layer in the wall-bounded region. The unbounded flow with negligible wall effect will be referred to as the self-preserving flow.

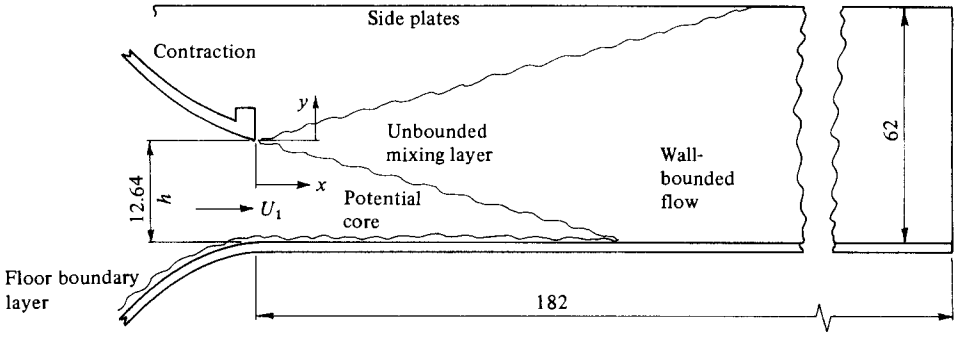


FIGURE 1. Schematic diagram of test rig. All dimensions in cm.

the influence of the wall became important, *all* the spanwise and streamwise correlation scales increased, and it was argued that this stretched and weakened the double-roller component. The most surprising result was that $\overline{v^2}$ was amplified significantly across the whole layer, in contrast with the intuitive and theoretical expectation (Hunt & Graham 1978; Wood & Ferziger 1983) that the wall should amplify $\overline{u^2}$ and $\overline{w^2}$ at the expense of $\overline{v^2}$. It was suggested that the rise in $\overline{v^2}$ was associated with an alteration to the fluctuating pressure field caused by the wall; the mean-velocity profile did not alter until the flow reached the floor.

A major motivation for the present work arose from the widely held view that any generally applicable turbulence model should simulate the structural differences between an unbounded shear layer and one constrained by a wall. For a thin shear layer, the most important differences occur in the $\overline{uv}$ transport equation, specifically in the turbulent-transport term $\overline{uv^2}$, which can be measured, and in the pressure–strain 'redistribution' term, which cannot. By analogy with the Poisson equation for the instantaneous pressure, it is now generally accepted that the latter should be modelled in two parts, one depending on the mean strain rate and the other depending only on the turbulence. Unfortunately the pressure term itself can only be deduced by difference after measuring all the other terms in the equation for $\overline{uv}$, and the two parts cannot, in general, be separated. The first effect of a solid surface on the fluctuating pressure field is to add a wall-reflection term, best thought of as an integral of the Poisson equation over the instantaneous image flow beneath the surface. The integral has a part depending on the mean strain rate of the image flow, but it clearly cannot be even approximately related to the mean strain rate at the point in the real flow where the pressure–strain term is required. The explicit wall-affected terms in some empirical turbulence models are generally functions of the ratio of the turbulence lengthscale, say $(\overline{q^2})^{\frac{3}{2}}/\epsilon$, where $\epsilon$ is the dissipation, to distance from the wall (e.g. Launder, Reece & Rodi 1975; Gibson & Launder 1978) and so are much too crude to be interpreted as image 'integrals'.

The present experimental techniques are the same as those described in I and more fully documented in Wood (1980). Since the hot-wire probes had to be moved upstream into the potential core for calibration and it was not possible to infer $\overline{uv}$-profiles from the measured mean-velocity distributions with the same accuracy as in I (see §2.1) to check the accuracy of the hot-wire measurements, the uncertainty in the present measurements, about 15% and 30% for the second- and third-order results respectively, is higher than for those in I. A comparison of measured and calculated $\overline{uv}$ in I suggests that the former are underestimated by about 10%.

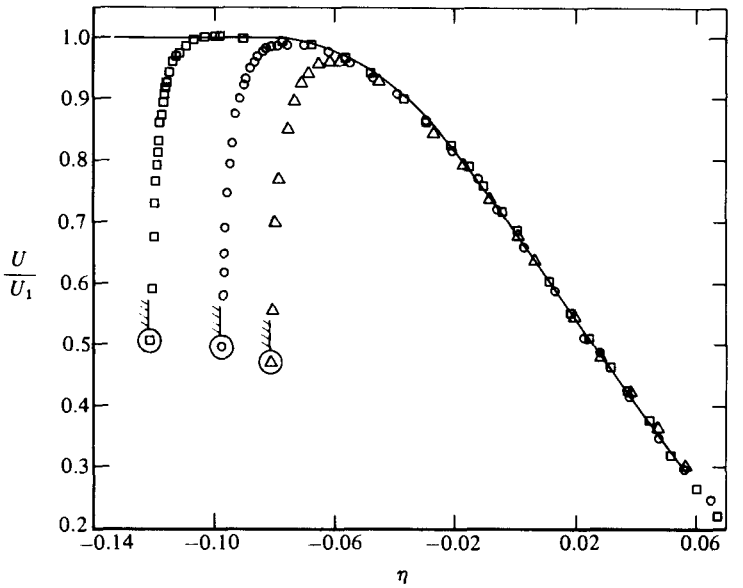


FIGURE 2. Mean-velocity profiles. $x-x_0$ (cm): □, 104.7; ○, 129; △, 155.6. Solid line is best fit to self-preserving profile. The position of the wall is indicated.

The results are presented in the same order as in I. In the absence of a suitable alternative we persist with mixing-layer similarity scaling for the results, that is $U_1$ ($= 16.4 \pm 0.1$ m s$^{-1}$) is the velocity scale and $x-x_0$ is the lengthscale, where $x_0 = -6.8$ cm is the position of the effective origin. The scaled position of the wall, denoted by $\eta_w$, where $\eta \equiv y/(x-x_0)$, is $-0.126$, $-0.100$ and $-0.0834$ at $x-x_0 = 100.38$, 125.9 and 151.1 cm respectively. Only the last two stations are in the wall-bounded flow. The 100 cm results are included to indicate typical values in the unbounded mixing layer. Any substantial changes that occurred *before* 100 cm will also be noted. The mean velocity and single-point turbulence measurements are given in §2, and the correlation results in §3. A general discussion follows in which the implications for calculation methods are considered.

## 2. Single-point results

The mean-velocity profiles are shown in figure 2 together with the fully developed distribution from I. The points closest to the wall, when fitted to the law of the wall, indicate that the skin-friction coefficient $c_f \equiv \tau_w/\frac{1}{2}\rho U_1^2$ was 0.0039 at both 126 and 152 cm. Away from the wall, the mean velocity hardly deviates from the unbounded distribution. The maximum value of the intermittency factor $\gamma$ in figure 3 continues the decrease with increasing $x$ that was noted in I. Near the wall $\gamma$ rises again and should reach unity deep within the wall 'boundary layer'. The local minimum in $\gamma$, perhaps the best definition for the boundary-layer edge, occurs at $\eta = 0.057$ and so is reasonably close to the position of maximum velocity, given in table 1.

The mean-square intensities are shown in figure 4 – note that the vertical scale for $\overline{u^2}$ is twice that for $\overline{v^2}$ and $\overline{w^2}$. In a zero-pressure-gradient boundary layer the maximum levels of $\overline{u^2}$, $\overline{v^2}$ and $\overline{w^2}$ are roughly 2.5, 0.5 and 1 times $u_\tau^2$ respectively. These levels are shown in figure 4 to demonstrate that the enormous rise in $\overline{u^2}$ and the lesser rise in $\overline{w^2}$ are caused by the effect of the wall on the mixing-layer turbulence. In contrast,

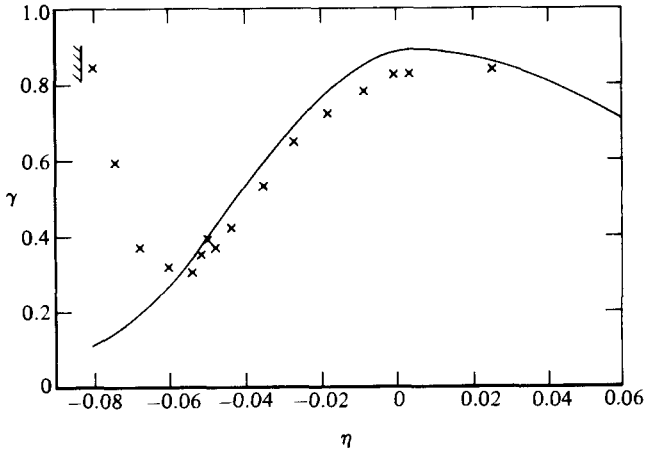


FIGURE 3. Intermittency factor at $x-x_0 = 151.5$ cm. Solid line shows the distribution at 75.06 cm.

| Quantity | $x-x_0$ (cm) | |
|---|---|---|
| | 129.87 | 151.51 |
| $\overline{uv}/U_1^2$ | −0.091 | −0.069 |
| $\partial U/\partial y$ | −0.078 | −0.062 |
| $\overline{q^2 v}$ | −0.080, −0.005 | −0.061, −0.010 |
| $\partial \overline{q^2}/\partial y$ | −0.080, −0.015 | −0.061, +0.014 |

TABLE 1. Position of zeros on high-velocity side

$\overline{v^2}$ hardly alters from its distribution at 100 cm probably because the expected decrease due to the wall acting on the mixing-layer turbulence is offset by the rise in $\overline{v^2}$ that normally occurs in a boundary layer as the wall is approached.†

Spectra of the $u$- and $v$-components are shown in figure 5 using the same scaling as in I, that is

$$\phi'_{ii}(\omega) \equiv \frac{U_1 \phi_{ii}(\omega)}{x-x_0},$$

where

$$\int_0^\infty \phi_{ii}(\omega)\,\mathrm{d}\omega = 1,$$

is plotted against the dimensionless radian frequency

$$\omega' \equiv \omega(x-x_0)/U_1$$

for $i = 1, 2$. As the wall is approached, $\phi_{11}$ develops a peak at $\omega \approx 10$ Hz, or $\omega' \approx 5.8$, the same frequency as the peak in all the $\phi_{22}$. Recall from I that the rise in $\overline{v^2}$ after $x-x_0 = 62$ cm was associated with the development of a strong peak in $\phi_{22}$ at about 8.5 Hz (or $\omega' \approx 2.4$ at 75 cm); at the same time $\phi_{11}$ developed a slight peak at the same frequency.‡

† Note that $\overline{v^2}$ in the unbounded flow increased from the self-preserving distribution shown in figure 4.

‡ A mistake was made in the computer plotting of $\phi_{11}$ and $\phi_{22}$ from which figures 5 and 6 of I were drawn. All the plotted points should be shifted to the left by the amount $\log_{10}[(i-\frac{1}{2})/(i+1)]$, where $i$ is the number of the point counting from the left. The mistake is significant only for the first eight points and the only subsequent error of any importance is in the peak value for $\omega'$, given as 3.6 in I; the correct value is 2.4. The spectra in figure 5 of this paper are plotted correctly.

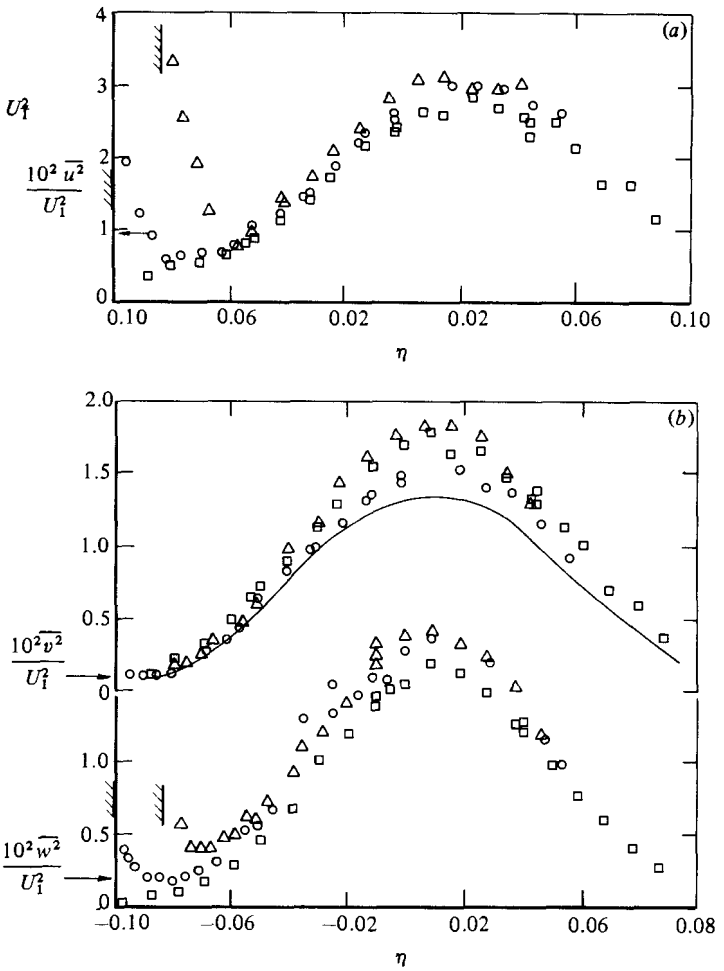


FIGURE 4. Normal stress profiles. $x-x_0$ (cm): □, 100.4; ○, 125.9; △, 151.5. The position of the wall is indicated. Horizontal arrows show boundary-layer normal-stress levels as explained in text. Solid line is self-preserving $\overline{v^2}$. (*a*) $\overline{u^2}/U_1^2$; (*b*) $\overline{v^2}/U_1^2$ and $\overline{w^2}/U_1^2$.

Since the difference between the peak frequencies at 75 and 152 cm is less than the frequency windows used to generate the spectra, it is possible that the peaks occur at the same frequency and so are associated with some form of upstream influence which would not scale on $x-x_0$. This possibility was discounted in I largely on the ground that the thin-shear-layer form of the turbulent-energy equation, which precludes upstream influence, provided a plausible explanation for the rise in $\phi_{22}$. We defer further discussion of the spectral peaks until the turbulent-energy balance is presented in §4.

The spectra measured closest to the wall appear to contain widely separated contributions from the mixing-layer and boundary-layer turbulence. In normal boundary layers there is a broad peak in $\phi_{ii}$ at around $\omega \approx U_1\delta_{\mathrm{bl}}^{-1}$. Assuming that the boundary-layer thickness $\delta_{\mathrm{bl}}$ is the distance from the wall at which $\gamma$ is a minimum gives $\log_{10}(U_1\delta_{\mathrm{bl}}^{-1}) \approx 1.8$. As $\omega'$ increases, the boundary-layer contribution increasingly dominates the rapidly diminishing mixing-layer component to the extent that an inertial subrange appears for the former. As a rough estimate of the contribution of

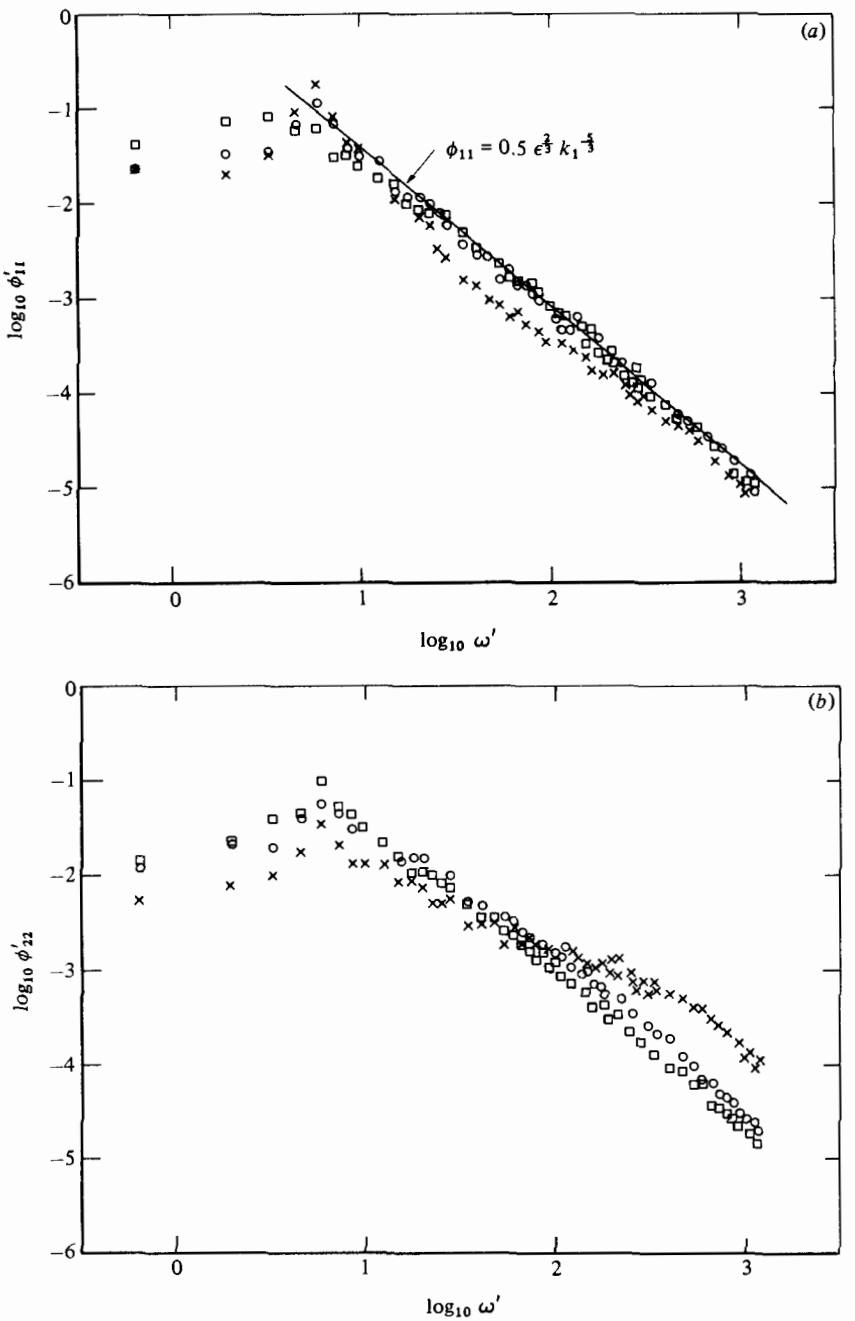


FIGURE 5. $\phi_{11}$ and $\phi_{22}$ at 151.5 cm: ×, $\eta = -0.0757$; ○, $-0.052$; □, $+0.014$. Solid line shows inertial-subrange equation at $\eta = +0.014$. (*a*) $\phi_{11}$; (*b*) $\phi_{22}$.

the boundary-layer turbulence to the normalized spectra, $\log_{10}\phi'_{ii}$ at $\log_{10}\omega' = 1.8$ is $-3.0$, $-2.6$ and $-2.8$ for $i = 1$, 2 and 3 respectively ($\phi_{33}$ was measured at $\eta = -0.0774$). Since the values are in inverse proportion to the degree of amplification by the wall, they are consistent with our earlier conclusion that the amplification of $\overline{u^2}$ and $\overline{w^2}$ was caused by the effect of the wall on mixing-layer turbulence, rather than by shear production in the boundary layer.

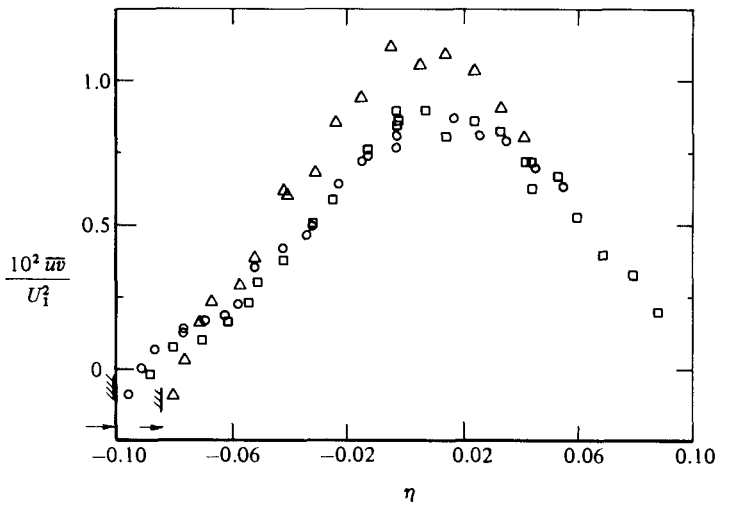


FIGURE 6. Shear-stress profiles. Symbols as in figure 4. Horizontal arrows show the wall shear stress at 125.9 and 151.5 cm inferred from the logarithmic law.

The measured shear-stress distributions are plotted in figure 6. Accurate profiles could not be obtained from the measured mean velocity using the momentum equation because of the difficulty in evaluating the normal-stress term $\partial(\overline{u^2}-\overline{v^2})/\partial x$. In the wall-bounded flow, this term was estimated as the difference between $\overline{u^2}-\overline{v^2}$ at the station where $\overline{uv}$ was required and that at the previous station. The calculations were started at 100 cm. The resulting maximum value of $\overline{uv}/U_1^2$ was $1.73\times10^{-2}$ at 152 cm, while ignoring the normal-stress term altogether gave a maximum value of $1.47\times10^{-2}$ at 152 cm. It will be shown in §4 that the streamwise component of the advection of turbulent energy, found in a similar manner to $\partial(\overline{u^2}-\overline{v^2})/\partial x$ is overestimated at 152 cm, especially near the wall, where both terms are dominated by $\overline{u^2}$. Thus $\partial(\overline{u^2}-\overline{v^2})/\partial x$, and hence $\overline{uv}$, are also likely to be overestimated at 152 cm. In any case, the calculations and measurements show a general increase in the level of $\overline{uv}$ after the flow reached the floor.

The $c_f$ values inferred from the mean velocity near the wall appear to be consistent with the hot-wire results. The position where $\overline{uv}$ passes through zero is closer to the wall than the point where $\partial U/\partial y = 0$ at both 126 and 152 cm as in a fully developed wall jet. Near the wall, the relatively high-wavenumber boundary-layer turbulence must be responsible for the shear-stress-producing motion, but $\overline{u^2}$ and $\overline{w^2}$ at least, and hence the bulk of the turbulent energy, are produced by mixing-layer eddies at relatively low wavenumber. In a normal boundary layer the analogue of the latter is called 'inactive motion' (Townsend 1961; Bradshaw 1967); the present flow, particularly at 152 cm, provides an extreme example of the disparity in scales induced by the wall that characterizes inactive motion.

It is shown in I that the flatness factors $F_u$ and $F_v$ on the high-velocity side decrease from approximately $3/\gamma$ to 3 as $x$ increases in the unbounded flow, with the most rapid decrease occurring in $F_u$. It was shown that the decrease was caused by the increasing fluctuation levels in the diminishing potential core of figure 1, see equations (4) and (5) of I. Figure 7 shows that $F_u$ hardly alters as the mixing layer reaches the floor, presumably because $F_u$ is no longer sensitive to the precise level of $\overline{u_N^2}/\overline{u_T^2}$, where T and N denote turbulent and non turbulent zone averages respectively. $F_v$ continues to decrease, partly because the increase in $\overline{v_N^2}$ in the unbounded flow was less than in $\overline{u_N^2}$ flow, so that $F_v$ can decrease after 100 cm as $\overline{v_N^2}$ increases.

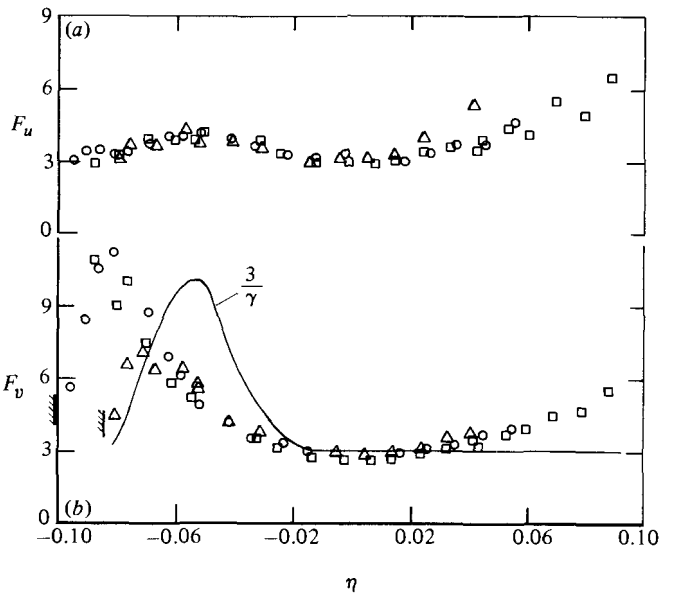


FIGURE 7. Flatness factor profiles. Symbols as in figure 4. Solid line is $3/\gamma$ at 151.5 cm. (*a*) $F_u$; (*b*) $F_v$.

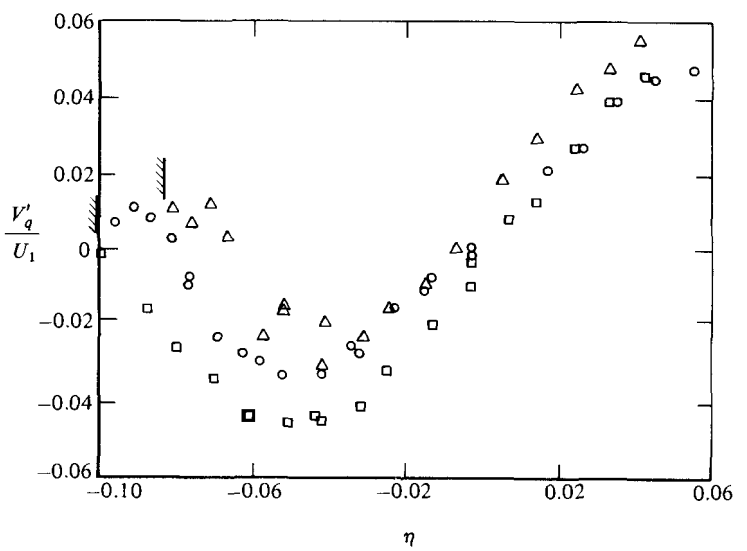


FIGURE 8. Turbulent-energy transport velocity. Symbols as in figure 4.

As in I, the triple products are presented in the abbreviated form of the transport velocities for turbulent energy and shear stress, after a brief description of the major changes in the individual triple products. The full results are given by Wood (1980). The decrease in magnitude of $\overline{u^3}$ on the high-velocity edge as $x$ increases continues into the wall-bounded flow; $\overline{u^3}$ finally becomes negative for $\eta \lesssim -0.06$ at 152 cm. The increase in magnitude of $\overline{v^3}$ near the potential core had finished by 100 cm, with $\overline{v^3}$ decreasing in magnitude after 100 cm, especially near the wall. Both $\overline{u^2v}$ and $\overline{uv^2}$ decrease in magnitude near the wall, with $\overline{uv^2}$ becoming negative in the region where

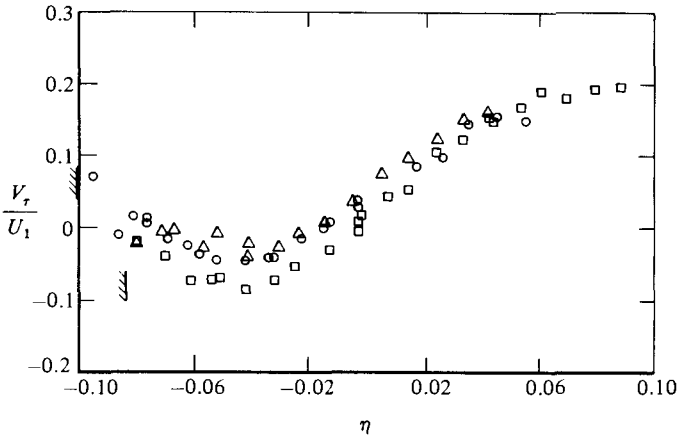


FIGURE 9. Shear-stress transport velocity. Symbols as in figure 4.

$\overline{uv}$ is also negative at 152 cm. The resulting transport velocities were found using the same approximation that $\overline{w^2v} \approx 0.2(\overline{u^2v}+\overline{v^2})$ as was used in I. They are

$$V'_q \equiv \frac{1.2(\overline{u^2v}+\overline{v^3})}{\overline{u^2}+\overline{v^2}+\overline{w^2}}, \quad V'_\tau \equiv \frac{\overline{uv^2}}{\overline{uv}},$$

and are shown in figures 8 and 9 respectively. It was found in I that, near the high-velocity edge, $V'_q$ decreased slightly in magnitude between 56 and 10 cm in the unbounded flow while $V_\tau$ was self-preserving at all stations except 100 cm, where there was also a decrease in magnitude, which was probably caused by experimental error. Near the high-velocity edge, the magnitude of $V'_q$ decreases significantly in the wall-bounded flow and becomes positive in the boundary-layer region. Since $V'_q$ is roughly constant and *positive* in the outer region of a boundary layer, with a value depending on the growth rate of the boundary layer (which we did not measure) (see e.g. Smits, Young & Bradshaw 1979), the positive $V'_q$ immediately adjacent to the wall is most likely due to the boundary-layer turbulence. In general, turbulent diffusion is affected by eddies of the same scale as the shear-layer thickness, so the large disparity in scale between the mixing-layer and the boundary-layer motion presumably also prevents any significant changes to the diffusion in the latter.

## 3. Two-point measurements and autocorrelations

Conditionally sampled two-point measurements, similar to those described in I, were also taken at 152 cm. However they appear to yield little information additional to that contained in the 'total' correlations, so only the latter are shown. The full measurements, taken with spanwise and normal separations, can be found in Wood (1980). At 152 cm the 'aspect ratio' of the shear layer, defined as the width of the wind tunnel, 76.2 cm, divided by the shear-layer thickness $\delta$, was about 2.5, so that the probe separation $r$ was limited to less than $\delta$ to avoid sidewall effects. We did not attempt to discriminate between boundary-layer and mixing-layer fluid, so that all the spanwise measurements were limited to the region where $\partial U/\partial y < 0$. Table 2 contains a summary of the spanwise correlations, with those at 37 and 75 cm included for comparison. The table gives the value of the correlation at the normalized probe separation indicated. The notation for the correlations is explained in I: for

| | $\eta = -0.05$ $r/(x-x_0) =$ | | | $\eta = -0.025$ $r/(x-x_0) =$ | | | $\eta = +0.025$ $r/(x-x_0) =$ | | |
|---|---|---|---|---|---|---|---|---|---|
| | 0.05 | 0.10 | 0.15 | 0.05 | 0.10 | 0.15 | 0.05 | 0.10 | 0.15 |
| | | | | $R_{11}(0,0,r)$ | | | | | |
| (*a*) | 0.15 | 0.08 | 0.08 | −0.05 | −0.04 | 0 | −0.05 | −0.02 | 0 |
| (*b*) | 0.30 | 0.22 | 0.21 | 0.10 | 0.01 | −0.02 | 0.10 | −0.02 | −0.02 |
| (*c*) | 0.43 | 0.32 | 0.29 | 0.08 | 0.05 | 0.07 | 0.11 | −0.03 | −0.03 |
| | | | | $R_{22}(0,0,r)$ | | | | | |
| (*a*) | 0.38 | 0.22 | 0.18 | 0.16 | 0.16 | 0.08 | 0.13 | 0.16 | 0.08 |
| (*b*) | 0.55 | 0.42 | 0.32 | 0.38 | 0.29 | 0.23 | 0.36 | 0.29 | 0.23 |
| (*c*) | 0.25 | 0.18 | 0.15 | 0.25 | 0.16 | 0.13 | 0.23 | 0.13 | 0.13 |
| | | | | $R_{12}(0,0,r)$ | | | | | |
| (*a*) | 0.34 | 0.15 | 0.12 | 0.07 | 0.06 | 0.07 | −0.04 | −0.03 | 0.03 |
| (*b*) | — | — | — | 0.27 | 0.22 | 0.20 | 0.22 | 0.11 | 0.08 |
| (*c*) | 0.34 | 0.32 | 0.30 | 0.15 | 0 | −0.04 | 0.15 | 0 | −0.04 |
| | | | | $R_{33}(0,0,r)$ | | | | | |
| (*a*) | 0.15 | −0.03 | −0.05 | 0.15 | −0.02 | −0.05 | — | — | — |
| (*b*) | 0.27 | 0.07 | −0.02 | 0.25 | 0.10 | −0.05 | — | — | — |
| (*c*) | 0.24 | 0.02 | −0.05 | 0.22 | 0.05 | −0.05 | 0.22 | 0.05 | −0.05 |

TABLE 2. Values of spanwise correlations at separations indicated. Nominal $x-x_0$ (cm): (*a*), 37; (*b*) 75; (*c*), 152.

| | $R_{11}(r',0,0)$ | | | $R_{22}(r',0,0)$ | | | $R_{33}(r',0,0)$ | | |
|---|---|---|---|---|---|---|---|---|---|
| $\eta$ | (*a*) | (*b*) | (*c*) | (*a*) | (*b*) | (*c*) | (*a*) | (*b*) | (*c*) |
| −0.0774 | — | — | — | — | — | — | 0.060 | 0.300 | −0.15 |
| −0.0757 | 0.135 | 0.275 | −0.350 | 0.110 | 0.200 | −0.06 | — | — | — |
| −0.052 | 0.140 | 0.270 | −0.225 | 0.120 | 0.240 | −0.13 | 0.150 | 0.300 | −0.016 |
| +0.014 | 0.205 | 0.360 | −0.105 | 0.130 | 0.230 | −0.18 | — | — | — |
| +0.018 | — | — | — | — | — | — | 0.120 | 0.220 | −0.09 |

TABLE 3. Properties of 'streamwise' correlations. Values are $r'/(x-x_0)$, where $r' = U_c t$ at (*a*) crossover point and (*b*) position of negative peak. (*c*) is *value* of negative peak.

example $R_{11}(0,0,r)$ is the spanwise correlation of the $u$-component, and the same definition of correlation scale is used: that is the scale is either the position where the correlation (whose maximum value is 1) has fallen to 0.05, or the crossover point before a negative region if any. The most noticeable feature of the results at 152 cm is the large increase in scale of $R_{11}(0,0,r)$ as the wall is approached, suggesting that the relatively low aspect ratio did not affect the eddy structure. At the same time, the scales of $R_{22}(0,0,r)$ and $R_{33}(0,0,r)$ do not alter significantly. At constant $\eta$, only the scale of $R_{22}(0,0,r)$ has decreased markedly from the value at 75 cm. $R_{12}(0,0,r)$ appears to be re-establishing the negative loop it had at 37 cm but had lost by 75 cm, and so is once again becoming similar in shape to $R_{11}(0,0,r)$.

As in I, the autocorrelations were converted into pseudostreamwise correlations by using $r' \equiv U_c t$, where $U_c$ is the convection velocity and $t$ is the time delay. For

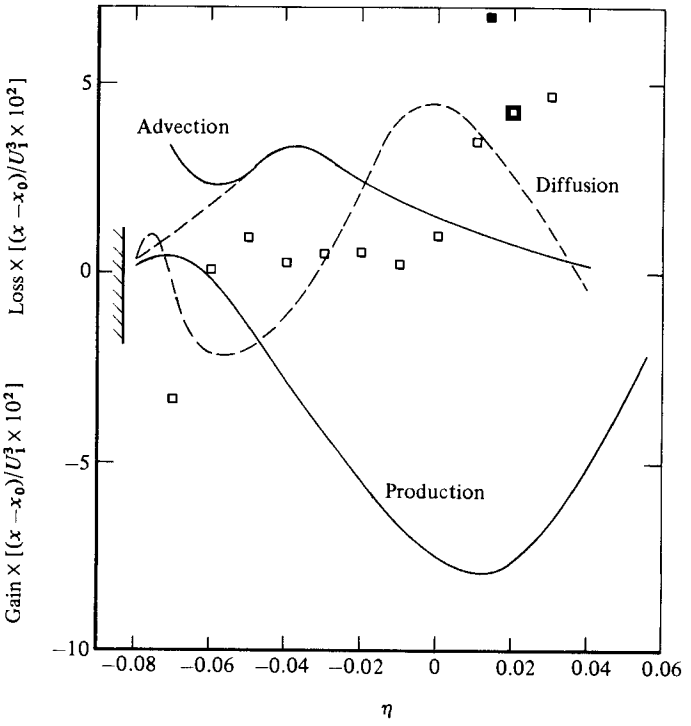


FIGURE 10. Balance of turbulent-energy equation at 151.5 cm. □, Dissipation by difference; ■, dissipation from inertial-subrange equation.

all three components $U_c$ was assumed to be the local mean velocity for $\eta \geqslant 0$, and $U(\eta = 0) = 0.675U_1$ for $\eta < 0$, following the unbounded-mixing-layer measurements of Wills (1964). The results are given in table 3 in the same form as in table 1 of I. All the streamwise correlations have decreased by 152 cm; for example at $\eta = -0.050$ the crossover point in $R_{ii}(r', 0, 0)$, which is entry $(a)$ in table 3, was 0.37, 0.30 and 0.20 for $i = 1$, 2 and 3 respectively at 75 cm. As the wall is approached, only $R_{11}(r', 0, 0)$ decreases significantly in scale, suggesting that the stretching of the eddies in the plane of the wall occurs mostly in the spanwise direction. The relative increase in $R_{11}(0, 0, r)$ over $R_{33}(0, 0, r)$ as the wall is approached is probably related to the relatively larger amplification of $\overline{u^2}$.

## 4. General discussion

The most interesting change in the turbulence structure as the mixing layer finally reaches the floor is the large rise in $\overline{w^2}$ and the huge rise in $\overline{u^2}$ adjacent to the surface, while $\overline{v^2}$ hardly alters, presumably because the attenuation of the mixing-layer motion is balanced by the increase in the boundary-layer component.

Since the overall level of $\overline{uv}$ has risen appreciably from the self-preserving level, while the mean velocity has hardly altered over most of the shear layer, the total production of turbulent energy (which is dominated by $\overline{uv}\,\partial U/\partial y$) increases, and hence the level of $\overline{q^2}$ must increase somewhere in the wall-bounded flow. Figure 10 shows the balance of turbulence energy (equation 10 $(d)$ of I) at 152 cm. The only significant $x$-dependent term, $U\partial\frac{1}{2}\overline{q^2}/\partial x$, which is the streamwise component of the advection, was approximated in the same way as the normal-stress term in the mean-momentum

equation, that is by using the difference between $\overline{q^2}$ at 152 and 126 cm. The resulting $U\partial\frac{1}{2}\overline{q^2}/\partial x$ dominates the advection close to the wall where $V$ is very small. From the negative values of the dissipation found by difference, it is obvious that the magnitude of $\partial\frac{1}{2}\overline{q^2}/\partial x$ has been grossly overestimated close to the wall, suggesting that the amplification of $\overline{u^2}$ and $\overline{w^2}$ is close to a maximum at 152 cm. A more plausible variation of the advection is shown in figure 10. In contradistinction to the energy balance in the unbounded flow, the measured $\overline{uv}$ rather than the values calculated from the mean-momentum equation were used to obtain the production. From I, the measured $\overline{uv}$ in the unbounded flow is around 10% too low, so that the magnitude of production in figure 10 is also likely to be low, as suggested by the disagreement – larger than found in I – between the dissipation found by difference and that obtained from the inertial subrange part of $\phi_{11}$ at $\eta = +0.014$ (see figure 5*a*). If the magnitude of the production was increased by around 10%, the resulting discrepancy between the two estimates of the dissipation would be about the same at 152 cm as in I. The discrepancy at 75 cm is no larger than at 37 cm, where there were no sharp spectral peaks which could be associated with feedback. Since the spectral determination of $\epsilon$ should be independent of the validity of the thin-shear-layer approximation to the turbulent-energy equation, it is unlikely that any significant feedback mechanism affected the results.

As would be expected from the different positions of zero $\overline{uv}$ and $\partial U/\partial y$ (table 1), the production of $\overline{q^2}$, which is mostly production of $\overline{u^2}$, is a loss close to the wall. It is likely that this 'negative' production near the wall occurs throughout the region $100 \leqslant x - x_0 \leqslant 153$ cm, so that the level of $\overline{q^2}$ is increased mostly by the advection and diffusion from regions of higher production. The redistribution of $\overline{q^2}$ which causes the rise in $\overline{u^2}$ and $\overline{w^2}$ is then directly attributable to the alteration of the pressure–velocity terms in the individual normal-stress equations (10(*a–c*) of I) by the wall; note that these redistributive terms sum to zero by continuity, and so have no effect on the level of $\overline{q^2}$. In I the behaviour of these terms was associated with the unexpected rise in $\overline{v^2}$ across the unbounded shear layer; it is remarkable that the expected redistribution of the normal stresses caused by the wall does not occur until after the mixing layer has made contact with the surface.

The balance of the terms in the shear-stress equation (equation (11) of I) at 152 cm is shown in figure 11. The pressure–strain was found by difference. Since the general rise in $\overline{uv}$ is smaller than that in $\overline{u^2}$ and $\overline{w^2}$, the mean transport, the only term in the $\overline{uv}$-equation that contains a streamwise derivative, should be more accurate than the advection of turbulent energy. Thus the mean transport is likely to be only slightly in error near the wall, so that the negative pressure–strain for $\eta \lesssim -0.06$ is at least qualitatively correct, as is the general decrease in the pressure–strain for $\eta \lesssim 0$ from that at 100 cm. Recall from I that the pressure–strain at 100 cm is *greater* than the self-preserving value for $\eta \gtrsim -0.03$, as the mean and turbulent transport did not increase sufficiently to absorb the extra generation caused by the rise in $\overline{v^2}$. At face value these non-monotonic changes would require the modifying functions appearing in current models for the effect of the wall on the pressure–strain (see §1) to be functions of $x$, as the turbulent lengthscale $(\overline{q^3})^{\frac{3}{2}}/\epsilon$ increases *monotonically* with $x$ in the region $0 \gtrsim \eta \gtrsim -0.05$.

The effect of the wall on the triple-product terms, $\overline{uv^2}$ in the $\overline{uv}$-equation, and $\overline{\frac{1}{2}q^2v}$ in the turbulent-energy equation, is easier to measure and assess. It is most simply expressed as a reduction in magnitude of both transport velocities, $V_{q'}$ and $V_\tau$ on the high-speed side, where they are directed towards the wall (figures 8 and 9). This reduction is related to the pressure fluctuations generated where the large eddies

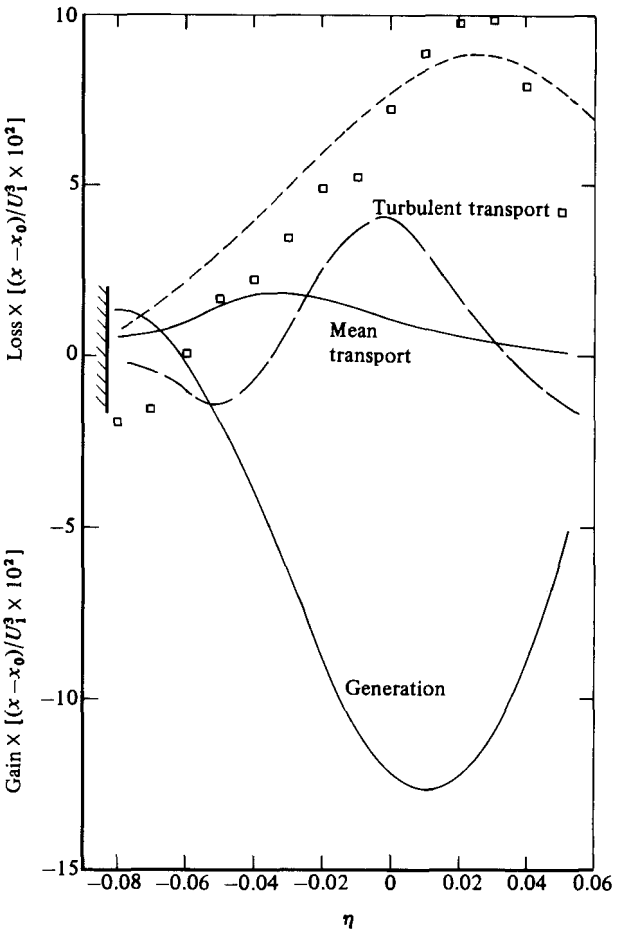


FIGURE 11. Balance of shear-stress equation. □, pressure–strain by difference. Dashed line is pressure–strain at 75.06 cm.

'impact' on the wall: presumably the mean-strain contribution does not have a first-order influence on this aspect of wall effect. There is also some evidence from perturbed boundary layers (e.g. Smits *et al.* 1979; Andreopoulos & Wood 1982) that the triple products in other rapidly changing flows cannot be adequately represented by any local formula for the transport velocity. A similar conclusion holds also for the diffusivities of $\overline{uv^2}$ and $\overline{q^2v}$, defined as $\overline{uv^2}/(\partial\overline{uv}/\partial y)$ and $\overline{q^2v}/(\partial\overline{q^2}/\partial y)$ respectively, which are more commonly used to model the triple products. Even though the diffusivities are well behaved in the wall-bounded flow, as $\overline{q^2v}$ and $\partial\overline{q^2}/\partial y$ both go through zero together (see table 1), both diffusivities decrease monotonically from the self-preserving value for $\eta \lesssim -0.010$. The *decrease* in each is by a factor of around 2 (the results are not shown), while $\overline{q^2}/\epsilon$, commonly used as the timescale in the various models for the triple products (see e.g. Cormack, Leal & Seinfeld 1978), monotonically *increases* for $0 \gtrsim \eta \gtrsim -0.05$ between 50 and 152 cm.

The general decrease in the $(r', 0, 0)$ correlation scales, which is associated with the small change in the dimensional peak spectral frequency between 75 and 152 cm, indicates that the stretching of the large eddies in the plane of the wall is self-limiting. This in turn suggests that the original average large-eddy structure from the

self-preserving flow has retained its identity, if not its shape, because the only way that a correlation scale can continue to grow more rapidly than the shear-layer thickness is by significant amalgamation of adjacent large eddies. It appears that by 152 cm the double-roller component is beginning to recover from being stretched and weakened by the initial effect of the wall at around 75 cm.

## 5. Conclusions

The measurements presented here complete the documentation of the response of a single-stream mixing layer to the imposition of a solid surface. The relative increase in the normal stresses in the plane of the wall occurs close to the wall in the wall-bounded flow, but only after there is a relative *increase* in $\overline{v^2}$ across the whole unbounded shear layer. The spectra and the comparison of the measured normal stresses to typical values in zero-pressure-gradient boundary layers confirm that the near-wall amplification of $\overline{u^2}$ and $\overline{w^2}$ is due directly to the effect of the wall on the mixing-layer turbulence. The wall apparently alters the pressure field and hence the redistribution terms in the individual normal stress equations causing a transfer of energy *to* $\overline{v^2}$ in the unbounded flow but transfer *from* $\overline{v^2}$ in the wall-bounded flow. In contrast, the magnitudes of the transport velocities for turbulent energy and shear stress and the corresponding diffusivities generally decrease monotonically with $x$ on the high-velocity side. However most models of the diffusivities involve $\overline{q^2}/\epsilon$, which increases with increasing $x$ over most of the high-velocity side.

The small shift in the dimensional frequency of the sharp spectral peak found at both 75 and 152 cm may be associated with some form of upstream feedback, although the approximate agreement between the dissipation found by difference and that inferred from the inertial-subrange equation suggests otherwise. The small change is more likely to be associated with some self-limiting of the size of the average large-eddy structure relative to the shear-layer thickness after the large increase that occurred by 75 cm. There is some evidence to suggest that the double-roller component of the large eddies is becoming more important by 152 cm after having been stretched and weakened by the initial influence of the wall.

The results suggest that a calculation method sufficiently sophisticated to stimulate the change from a free shear layer to a wall-bounded one would have to include non-local formulae for the triple products. Furthermore the complex non-monotonic changes to the relative distribution of the turbulent energy among its three components indicates the need to provide equations for each normal stress, if for no other reason than that $\overline{v^2}$ is the only normal stress that appears in the generation term for the shear stress. However the inclusion of the effect of the wall on the pressure-containing terms in the normal-stress equations and the $\overline{uv}$-equation is probably the most difficult requirement to achieve.

This work was funded by S.R.C. Grants B/SR/8978.1 and B/RG/9011.2. We also thank Professor J. H. Ferziger, Dr R. D. Mehta and Dr A. J. Yule for their valuable comments during the course of this work. We are grateful to Messrs D. Abrahams and P. N. Inman and Drs P. H. Hoffmann and Muck Kin-Choong for their help with the data reduction.

## REFERENCES


ANDREOPOULOS, J. & WOOD, D. H. 1982 *J. Fluid Mech.* **118**, 143.

BRADSHAW, P. 1967 *J. Fluid Mech.* **30**, 241.

BRADSHAW, P. 1975 *Trans. ASME* I: *J. Fluids Engng* **97**, 146.

BRADSHAW, P. 1976 In *Proc. 14th Intl Congr. Appl. Mech.* (ed. W. T. Koiter), p. 101. North-Holland.

CORMACK, D. E., LEAL, L. G. & SEINFELD, J. H. 1978 *Trans. ASME* I: *J. Fluids Engng* **100**, p. 47.

GIBSON, M. M. & LAUNDER, B. E. 1978 *J. Fluid Mech.* **86**, 441.

GRANT, H. L. 1958 *J. Fluid Mech.* **4**, 149.

HUNT, J. C. R. & GRAHAM, J. M. R. 1978 *J. Fluid Mech.* **84**, 209.

KLINE, S. J., CANTWELL, B. J. & LILLEY, G. M. (eds.) 1982 *Proc. 1981 Stanford Conf. on Complex Turbulent Flows*, vol. II.

LAUNDER, B. E., REECE, G. J. & RODI, W. 1975 *J. Fluid Mech.* **68**, 537.

SMITS, A. J., YOUNG, S. T. B. & BRADSHAW, P. 1979 *J. Fluid Mech.* **94**, 209.

THOMAS, N. H. & HANCOCK, P. E. 1978 *J. Fluid Mech.* **82**, 481.

TOWNSEND, A. A. 1961 *J. Fluid Mech.* **11**, 97.

WILLS, J. A. B. 1964 *J. Fluid Mech.* **20**, 417.

WOOD, D. H. 1980 A reattaching, turbulent thin shear layer. Ph.D. thesis, Imperial College, London.

WOOD, D. H. & BRADSHAW, P. 1982 *J. Fluid Mech.* **122**, 57.

WOOD, D. H. & FERZIGER, J. H. 1983 The potential flow bounded by a mixing layer and a solid surface. *Univ. Newcastle, Mech. Engng Dept. T.N.-F.M.* 83/5, and *Imperial College Aero TN* 83–104.